TOXICOLOGICAL SCIENCES **131(2)**, 537–547 2013
doi:10.1093/toxsci/kfs306
Advance Access publication October 19, 2012

Effects of Silver Nanoparticles on the Liver and Hepatocytes *In Vitro*

Birgit K. Gaiser,*[,1] Stephanie Hirn,† Ali Kermanizadeh,* Nilesh Kanase,* Kleanthis Fytianos,* Alexander Wenk,† Nadine Haberl,† Andrea Brunelli,‡ Wolfgang G. Kreyling,† and Vicki Stone*

**Heriot-Watt University, School of Life Sciences, Nanosafety Research Group, Edinburgh, EH14 4AS, UK; †Comprehensive Pneumology Center—Institute of Lung Biology and Disease, and Focus Network Nanoparticles and Health, Helmholtz Zentrum München—German Research Center for Environmental Health, Neuherberg, Germany; and ‡Department of Environmental Sciences, Informatics and Statistics, University Ca' Foscari Venice, 30123 Venice, Italy*

[1]To whom correspondence should be addressed at Heriot-Watt University, School of Life Sciences, NanoSafety Research Group John Muir Building, Edinburgh, EH14 4AS, UK. Fax: +44 (0)131 4513009. E-mail: b.gaiser@hw.ac.uk.

Received July 19, 2012; accepted October 13, 2012

With the increasing use and incorporation of nanoparticles (NPs) into consumer products, screening for potential toxicity is necessary to ensure customer safety. NPs have been shown to translocate to the bloodstream following inhalation and ingestion, and such studies demonstrate that the liver is an important organ for accumulation. Silver (Ag) NPs are highly relevant for human exposure due to their use in food contact materials, dietary supplements, and antibacterial wound treatments. Due to the large number of different NPs already used in various products and being developed for new applications, it is essential that relevant, quick, and cheap methods of *in vitro* risk assessment suitable for these new materials are established. Therefore, this study used a simple hepatocytes model combined with an *in vivo* injection model to simulate the passage of a small amount of NPs into the bloodstream following exposure, e.g., via ingestion or inhalation, and examined the potential of Ag NPs of 20 nm diameter to cause toxicity, inflammation, and oxidative stress in the liver following *in vivo* exposures of female Wistar rats via iv injection to 50 µg of NPs and *in vitro* exposures using the human hepatocyte cell line C3A. We found that Ag NPs were highly cytotoxic to hepatocytes (LC_{50} lactate dehydrogenase: 2.5 µg/cm^2) and affected hepatocyte homeostasis by reducing albumin release. At sublethal concentrations with normal cell or tissue morphology, Ag NPs were detected in cytoplasm and nuclei of hepatocytes. We observed similar effects of Ag NPs on inflammatory mediator expression *in vitro* and *in vivo* with increase of interleukin-8 (IL-8)/macrophage inflammatory protein 2, IL-1RI, and tumor necrosis factor-α expression in both models and increased IL-8 protein release *in vitro*. This article presents evidence of the potential toxicity and inflammogenic potential of Ag NPs in the liver following ingestion. In addition, the similarities between *in vitro* and *in vivo* responses are striking and encouraging for future reduction, refinement, and replacement of animal studies by the use of hepatocyte cell lines in particle risk assessment.

Key Words: **nanoparticles; metals; hepatocytes; *in vitro* alternatives; liver toxicology.**

Silver nanoparticles (Ag NPs) are incorporated into consumer products primarily due to their antibacterial and antifungal properties. In 2011, more than 300 products containing nanosilver were on the market (http://www.nanotechproject.org/inventories/consumer/analysis_draft/). Many of these products are designed for use in contact with the human body, such as clothes made of Ag NP-containing fabric (Kulthong *et al*., 2010) and personal hygiene products (Chao *et al*., 2011). Some are aerosolized, e.g., in air sanitizers or nasal sprays (Chao *et al*., 2011). Others again include wound dressings (Silver *et al*., 2006), nanosilver toothpastes, and colloidal silver suspensions designed as nutritional supplements (Nowack *et al*., 2011).

Although direct exposure of most organs to nanomaterials through the bloodstream is unlikely except in medical applications, there is potential for NPs to reach the bloodstream through inhalation (Mühlfeld *et al*., 2008), through the skin (Korani *et al*., 2011), or via the gastrointestinal tract (Schleh *et al*., 2012). For any exposure routes involving translocation to the bloodstream, the liver is one of the most important targets, and previous studies have shown a high accumulation of NPs in the liver after injection (Hirn *et al*., 2011), retention of particles in the liver after ingestion (Schleh *et al*., 2012), and effects on the liver following inhalation (Gosens *et al.*, in preparation). The liver was, therefore, chosen as a target organ in this study to identify adverse effects of nanoparticles should they gain access to the blood.

The increased use of nanomaterials, and exposure of humans and the environment, necessitates the availability of reliable, cost- and time-effective screening mechanisms for NP toxicology. As animal studies are cost and time intensive and there is additional pressure from regulators and the public to reduce their number, the search for suitable *in vitro* models to accurately predict toxicity *in vivo* is a research priority in the field of NP risk assessment (Stone *et al*., 2009). This study investigates various *in vitro* assays that could be used to reduce and potentially replace *in vivo* studies in the future and be included in the development of a more complex and physiological multitissue *in vitro* fluidic model developed in the FP7 project InLiveTox (www.inlivetox.eu).

Ag NPs have been shown to be highly toxic not only to bacteria and fungi but also to a number of animal species and cultured cells (Gaiser *et al*., 2012; Johnston *et al*., 2010). Ag toxicity has often been associated with ion release and induction of oxidative stress (Johnston *et al*., 2010). However, there have also been studies showing a higher toxicity of Ag NPs compared with the equivalent concentration of soluble silver (Powers *et al*., 2011), and particles with very low solubility have elicited high toxicity in exposed species and cells (Gaiser *et al*., 2012). The literature shows examples for both inflammatory (Nishanth *et al*., 2011) and anti-inflammatory (Wong *et al*., 2009) effects of nanosilver, as well as conflicting results with regards to the ability of Ag NPs to cause oxidative stress (Nishanth *et al*., 2011; Powers *et al*., 2011). Factors that can cause these conflicting results include the physicochemical characteristics of the NPs, such as size, shape, and solubility, and also the choice of model, exposure times, and concentrations. Therefore, it is very important that appropriate *in vitro* models and conditions are chosen to closely reflect *in vivo* toxicology, in particular with a view to finding feasible, but accurate, models for rapid and systematic screening of the hundreds of NPs already on the market and any new particles currently being developed.

For this particular study, *in vivo* exposures to NPs were conducted via the lateral tail veins of rats. The authors are currently conducting further studies exploring the pulmonary and gastrointestinal routes of exposure to compare the impact of particles on a set of target organs when applied by different routes. The human hepatoblastoma cell line C3A was used for *in vitro* assays. The endpoints investigated in this study include histopathology and electron microscopy of tissue from female Wistar rat livers and C3A hepatocytes, cytotoxicity and cell function *in vitro*, analysis of oxidative stress *in vivo* and *in vitro*, and the influence of nano-Ag on inflammatory gene expression and release of proinflammatory mediators in tissue and cell culture. Additionally, we hope that the results of this study will contribute to choosing suitable endpoints for *in vitro* risk assessment of other NPs, e.g., particles used in nanomedicine, which may be injected directly into the bloodstream and reach the liver in significant concentrations.

MATERIALS AND METHODS

Experimental design. We propose the hypothesis that simple *in vitro* models can be used to predict specific endpoints to NP exposure of the liver, such as particle uptake, expression of inflammatory mediators, and glutathione (GSH) expression. In this study, a low dose (50 µg) of NPs was injected into the tail vein of female Wistar rats to simulate particle exposure via translocation following ingestion or inhalation or dermal exposure such as in the case of silver-containing wound dressings being applied to abraded skin.

Animals. Experiments were conducted under German federal guidelines for laboratory animal use and care and approved by the Government of District of Upper Bavaria (Approval No. 55.2-1-54-2531-26-10) and the Institutional Animal Care and Use Committee of the Helmholtz-Zentrum in Munich, Germany. Female Wistar Kyoto rats (WKY/Kyo@Rj; Janvier, Le Genest Saint Isle, France), 8–10 weeks old (190–210 g body weight), were housed in pairs on a 12-h day/night cycle in humidity- and temperature-controlled ventilated cages. A rodent diet and water were provided *ad libitum*. Three animals per treatment group were used, and all animals were free of clinical symptoms throughout the 24 h exposure.

Particles and particle characterization. NM300 is one of the representative manufactured nanomaterials included in the OECD's Working Party on Manufactured Nanomaterials Sponsorship Programme and has, therefore, been chosen for investigation in a number of European projects such as InLiveTox (www.inlivetox.eu) and ENPRA (www.enpra.eu) in order to allow comparison of data across multiple projects and models. NM300 is a colloidal 10% wt/wt dispersion of Ag NPs in water containing 4% (wt/wt) each of polyoxyethylene glycerol trioleate and Tween 20 (Klein *et al*., 2011). NM300 and the NP-free dispersant control, NM300-DIS, were obtained from Mercator GmbH.

Ag NPs were characterized in the original suspension and in cell culture medium by electron microscopy, particle tracking analysis, dynamic light scattering (DLS), x-ray diffraction spectroscopy and inductively coupled plasma-optical emission spectrometry (ICP-OES) as described in Klein *et al*. (2011) and Kermanizadeh *et al*. (2012), and the results are summarized in Table 1.

Particles were purchased as suspensions, and information on synthesis methods or surface area measurements by BET prior to suspension was not provided by the suppliers. Because BET measurements cannot be carried out on suspended particles and the particles do not have completely regular shape, surface and particle number doses can only be estimated. Assuming the mean diameter of 17.3 nm and perfectly round shape, the particle number would be approximately 3.5×10^{10} particles/µg, and the surface area would be approximately 33.1 m^2/g; however, these values are purely based on estimation and cannot represent the actual size distribution, shape, and irregularities in the particle surface, which is reflected in the rather low surface area for a particle that size, so that particle mass will be used throughout this study rather than surface area or particle number.

The determination of impurities in NM300 was performed as follows: 0.1 ml of NM300 was taken from the vial by a syringe and transferred into a Teflon-lined, reaction vessel, which protected the sample from excessive outer pressure by using a special cap (Autovent Plus) during microwave digestion. An HNO_3 acid solution was then added into the vessel in order to obtain a complete sample mineralization. After sealing, the vessel was put into the rotor of an Ethos 1600 (Milestone, Shelton, CN) microwave oven. Power and time of digestion were selected as follows: 250 W for 5 min; 0 W for 1 min; 500 W for 5 min. After the digestion process, the reaction vessel was allowed to cool until room temperature (RT) under chemical hood for 2 h. The obtained acid solution was then transferred into a 25-ml Teflon flask. The digested sample was subsequently diluted with MilliQ water up to 25 ml. The diluted solution was then transferred into a Teflon bottle. Silver and other elements were analyzed by an Optima 5300 DV (PerkinElmer, Waltham, MA) Inductively Coupled Plasma-Optical Emission Spectrometry (ICP-OES).

Cells and cell culture. C3A cells (ATCC, Manassas, VA) were maintained as described in Gaiser *et al*. (2012), using M2279 medium (Sigma) supplemented with 10% fetal calf serum (FCS), 2mM L-glutamine, 100 U/ml penicillin/0.1 mg/ml streptomycin, 1mM sodium pyruvate, and 1% nonessential amino acids (all Sigma) at 37°C and 5% CO_2. For experiments, cells were plated on surfaces pretreated with 0.1 mg/ml of type I collagen from rat tails (Sigma-Aldrich).

Nanoparticle preparation and exposures. For *in vitro* exposures, particle suspensions were prepared by sonicating in a water bath for 16 min in water containing 2% FCS as described by Kermanizadeh *et al*. (2012). For *in vivo* application of Ag NPs, suspended particles were diluted with NM300-DIS to contain 1 µg/µl Ag NPs. Size distributions of the diluted Ag NPs were measured using DLS. Rats were anaesthetized by inhalation of 5% isoflurane until muscular tonus relaxed and kept under anaesthesia, whereas a flexible iv catheter (24G, 0.75 in) was placed into the tail vein. Fifty micrograms (238–263 µg/kg) of Ag NPs or dispersant were injected in the catheterized tail vein. After

TABLE 1
Physicochemical Characterization of Ag NM300 Nanoparticles

Characterization method	Conditions	Results	Notes and references
Transmission electron microscopy (carried out at different institutes with different vial numbers)	Original suspension Original suspension diluted 1:90 (nanopure water)	Modal diameter 1: 5.42 ± 1.72 nm Modal diameter 2: 15.03 ± 1.13 nm Mean diameter (small fraction not measured): 17.24 ± 3.17 nm Median diameter: 16.89 ± 1.90 nm	Klein *et al.* (2011)
Scanning electron microscopy	Original suspension	Modal diameter (small fraction not measured): 14.04 ± 1.35 nm	Klein *et al.* (2011)
Nanoparticle tracking analysis	1:1000 dilution in nanopure water	Mean diameter: 52.31 ± 25.99 nm Median diameter: 47 ± 17.79 nm	Klein *et al.* (2011); difference between mean and median indicates particles are not perfectly round
X-ray diffraction spectroscopy	Wet samples Dried samples	Mean diameter: 7 nm Mean diameter: 14 nm	Kermanizadeh *et al.* (2012)
TEM analysis	Original suspension	Mean diameter: 17.5 nm (size range: 8–47 nm)	Kermanizadeh *et al.* (2012)
DLS (hydrodynamic diameter)	Cell culture medium (10% serum) Diluted particles in NM300 dispersant for *in vivo* study	Fractions of particles at 12, 28, and 114 nm modal diameter Mean diameter: 28.48 nm, modal diameters 4.6 and 50.6 nm	Kermanizadeh *et al.* (2012); results indicate some degree of aggregation Characterization as part of this study
Solubility	Deionised water 0.1, 16, 128 µg/ml Cell culture medium (10% serum) 0.1, 16, and 128 µg/ml	Solubilities of < 0.01, 0.78, and 0.59%, respectively Solubilities of < 0.01, 0.19, and 0.47%, respectively	Kermanizadeh *et al.* (2012)
Inorganic impurities	0.1 ml of sample diluted in a tailored acid mixture and MilliQ water	Ca: 187 µg/l Fe: µg/l Zn: µg/l	Characterization as part of this study

24 h, animals were sacrificed by exsanguination under isoflurane anaesthesia. In all studies, NM300-DIS was applied at concentrations equivalent to the amount present in the highest dose of NP treatment.

The *in vivo* dose, 50 µg NPs per animal, corresponds to approximately 0.25 µg/10^6 hepatocytes based on available literature regarding liver cell numbers and particle retention in the liver following iv exposure. The *in vitro* doses used for initial exposures were slightly higher than this starting at 1.95 µg/10^6 cells, but taking into account the sedimentation rate of NM300 in cell culture media (< 10% over 24 h; Prof. Arti Ahluwalia, Univ. of Pisa, personal communication), the lower end of the concentration rage applied corresponds very well to the *in vivo* exposure.

AlamarBlue and lactate dehydrogenase assays. C3A cells were plated at a density of 300,000 cells/cm^2 and left to grow to confluence overnight. Confluent cells were exposed to 0–625 µg/cm^2 of Ag NPs and dispersant or 0.1% Triton X-100 for 24 h. Cell culture supernatants were removed for lactate dehydrogenase (LDH) analysis, cells were rinsed with PBS, and fresh medium containing 10% alamarBlue reagent (Invitrogen) was added. Cells were incubated at 37°C and 5% CO_2 for 90 min, before fluorescence was measured on a fluorescent plate reader (FLUOstar Optima, BMG Labtech) (544/590 nm). Supernatants were centrifuged (10 min, 10,000 × g) to remove cell debris and analyzed for LDH activity as described in Brown *et al.* (2001).

Albumin quantification. C3A cells were plated at a density of 300,000 cells/cm^2 and left to grow to confluence overnight. Confluent cells were exposed to cell culture medium containing 0 and 20% FCS as inhibitors and enhancers of albumin release, 1, 2, and 4 µg/cm^2 of Ag NPs, and 3.6 µg/cm^2 of dispersant for 24 h. Albumin was quantified in cell culture supernatants using the Human Albumin ELISA Quantitation Set (Bethyl Laboratories) according to the manufacturer's instructions. Samples were diluted 1:200 in assay diluent, and the dilution of the detection antibody was 1:16,667.

Confocal microscopy. Cells were seeded at low densities (4 × 10^4 cells/cm^2) on collagen-coated glass coverslips and left to adhere overnight. Medium was removed and replaced by fresh medium containing 1 µg/cm^2 NM300. After 24 h of exposure medium was removed, cells were washed in PBS and fixed in 4% *p*-formaldehyde in PBS. Fixed cells were permeabilized (0.2% Triton X-100 in PBS) and incubated with TRITC-conjugated phalloidin (Sigma-Aldrich). Coverslips were mounted on microscopy slides using Vectashield (Vector Laboratories). Slides were examined using a Zeiss LSM510 Meta confocal microscope and LSM510 Meta v3.2 SP2 software. Ag NPs were visualized by reflexion of light at 550 nm (Gaiser *et al.*, 2012).

Histology. Right lateral liver lobes of rats exposed to Ag NPs or dispersant were rinsed in 10% formaldehyde in PBS and transferred to a vial containing 10% formaldehyde in PBS for fixation. Fixed samples were sent to Histologix Ltd (Nottingham, UK) for embedding, sectioning, and hematoxylin/eosin (H&E) staining according to standard protocols.

Transmission electron microscopy. Transmission electron microscopy (TEM) images were captured on a Tecnai TF20 field emission gun transmission electron microscope. Where particles were detected, chemical composition was confirmed by energy-dispersive x-ray spectroscopy (EDX).

Confluent C3A cells were exposed to 5 µg/cm^2 NM300 particles for 4 h, washed with fresh medium, trypsinized, and centrifuged in BEEM capsules for 5 min (1000 × g), before being fixed in 2.5% glutaraldehyde in PBS for 2 h. Cubes of 2 mm side length were cut from the left lateral liver lobes of Ag NP–exposed rats, immersed in 2.5% glutaraldehyde (100mM phosphate buffer) for 2–3 h, and transferred into fresh phosphate buffer. Cell culture and liver samples were prepared for transmission electron spectroscopy at the University of Edinburgh's Biology department according to standard protocols.

GSH quantification. Reduced GSH in cell cultures was quantified according to the protocol of Senft *et al.* (2000). Briefly, cells seeded at 300,000 cells/cm^2 and exposed to particles for 2, 6, and 24 h after reaching confluence were scraped into PBS, centrifuged, lysed in a redox-quenching buffer, and GSH in the lysates was measured by fluorescence (350/420 nm; Spectramax M5, Molecular Devices) after reaction with *o*-phthalaldehyde (Sigma-Aldrich). GSH was normalized to protein content of the cell cultures as measured by the Bradford assay (Bradford, 1976).

Approximately, 0.5 g of the left lateral liver lobes of exposed rats was shock frozen in liquid nitrogen and stored at −80°C before homogenization (PowerGen 125, Fisher Scientific) in redox-quenching buffer (Senft *et al.*, 2000) containing 5% trichloroacetic acid on ice. Homogenates were incubated on ice for 15 min before further processing according to Senft *et al* (2000). Lysates were diluted 1:20 for analysis, and GSH content was normalized to tissue mass.

RNA isolation, RT reaction, and PCRs. Between 0.2 and 0.5 g of the left lateral liver lobe were minced, immersed in a tube containing RNAlater reagent (Ambion), and stored at −20°C until RNA isolation took place. Samples were homogenized in liquid nitrogen using a mortar and pestle. Homogenized tissues were stored at −80°C for up to 3 weeks before RNA was extracted and isolated using the MagMAX-96 Total RNA Isolation Kit (Ambion). C3A cells exposed to 0.1, 0.5, and 1 µg/cm^2 of NM300 and 1 µg/cm^2 of NM300-DIS for 4 and 24 h were lysed and processed according to the MagMAX protocol.

RNA concentration and purity were measured on a NanoDrop 2000c system (Thermo Scientific, UK). The High Capacity cDNA RT kit (Applied Biosystems, UK) was used according to the protocol to transcribe RNA into cDNA. Equal quantities of RNA from 3 to 4 animals in the same treatment group, or from three repeats of the cell culture exposures, were pooled, and 300 ng (livers) or 100 ng (cell cultures) of RNA were used in RT reactions.

PCRs were conducted in triplicate on a 7900 HT Fast Real-Time PCR System and SDS 2.3 software in 384-well plates (all Applied Biosystems), using TaqMan kits with FAM dye under standard TaqMan conditions for 50 cycles. The following Applied Biosystems kits were used:

In vivo (rat) kits: Rn00562055_m1 (tumor necrosis factor-α, TNF-α), Rn00580432_m1 (interleukin 1 beta, IL-1β), Rn00565482_m1 (IL-1 receptor IL-1RI), Rn00586403_m1 (chemokine cxcl2, macrophage inflammatory protein 2, MIP-2), Rn00569886_m1 (complement regulatory protein, monocyte chemotactic protein 1, MCP-1), Rn00563409_m1 (IL-10), Rn00577994_g1 (glutathione peroxidase, GSHpox), Rn00563754_m1 (FAS ligand, FasL), Rn00564227_m1 (intercellular adhesion molecule 1, ICAM-1), and Rn01775763_g1 (glyceraldehyde-3-phosphate dehydrogenase, GAPDH).

In vitro (human) kits: Hs02758991_g1 (GAPDH), Hs01555410_m1 (IL1β), Hs00991010_m1 (IL-1RI), Hs00961622_m1 (IL-10), Hs00174128_m1 (TNF-α), Hs00174103_m1 (IL8), and Hs00234140_m1 (ccl2, MCP-1).

FACSArray analysis of soluble mediators. Culture medium of C3A cells exposed to 1, 2, and 4 µg/cm^2 of Ag NPs and 4 µg/cm^2 of NM300-DIS was harvested 4 and 24 h after exposure and stored at −80°C. Samples were analyzed using the BD FACSArray with Flex Sets for human TNF-α (558273), IL8 (558277), FasL (558330), and ICAM-1 (560269) according to the instrument and Flex Set manuals.

Statistics and software. For statistical analysis, data were checked for normal distribution and processed using Minitab 15 software with ANOVA followed by *t*-test (significance: 95%). PCR results were analyzed using SDS 2.4, RQ Manager 1.2.1, and DataAssist 2.0 (all Applied Biosystems). A 1.8-fold increase or decrease in gene expression was used as cutoff value as reported in other such studies (e.g., Cheng *et al.*, 2007).

RESULTS

Cytotoxicity of Ag NPs in C3A Cells and Effect of Sublethal Ag Concentrations on Hepatocyte Homeostasis

Ag NPs were highly toxic to C3A cells *in vitro*, as determined after 24 h of exposure by two methods: The LDH assay measures activity of released LDH enzyme from damaged membranes, whereas the AlamarBlue assay measures

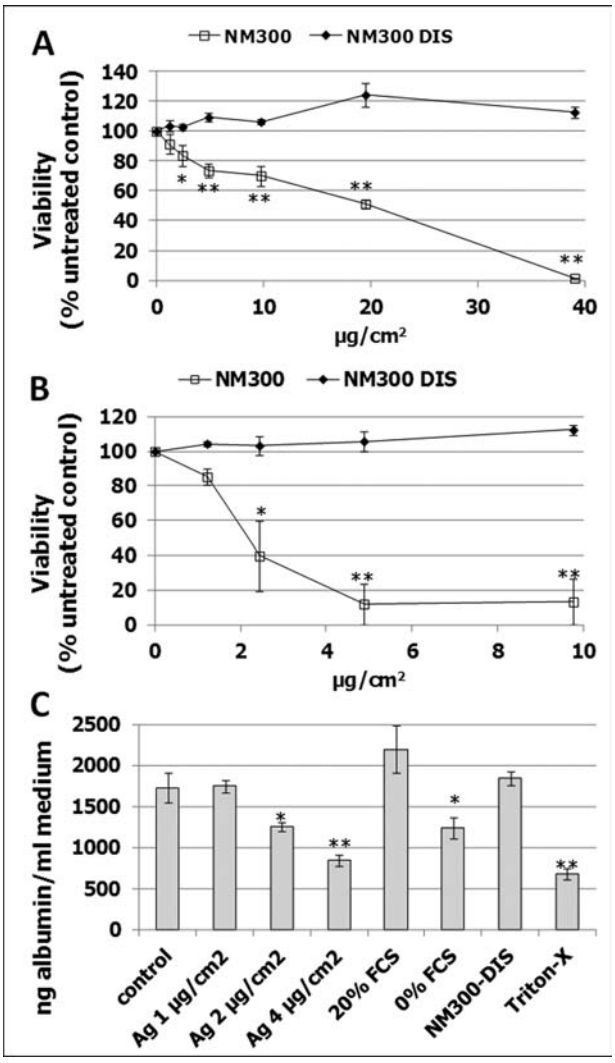

FIG. 1. Cytotoxicity and albumin release: C3A cells were exposed to Ag NPs NM300 and dispersant NM300-DIS for 24 h. Cytotoxicity was determined by AlamarBlue (A) and LDH (B) assays, and albumin in cell culture was measured by ELISA (C). Data represent means ± SEM, $n = 3–4$, $^{*}p < 0.05$, $^{**}p < 0.01$ (ANOVA followed by *t*-test).

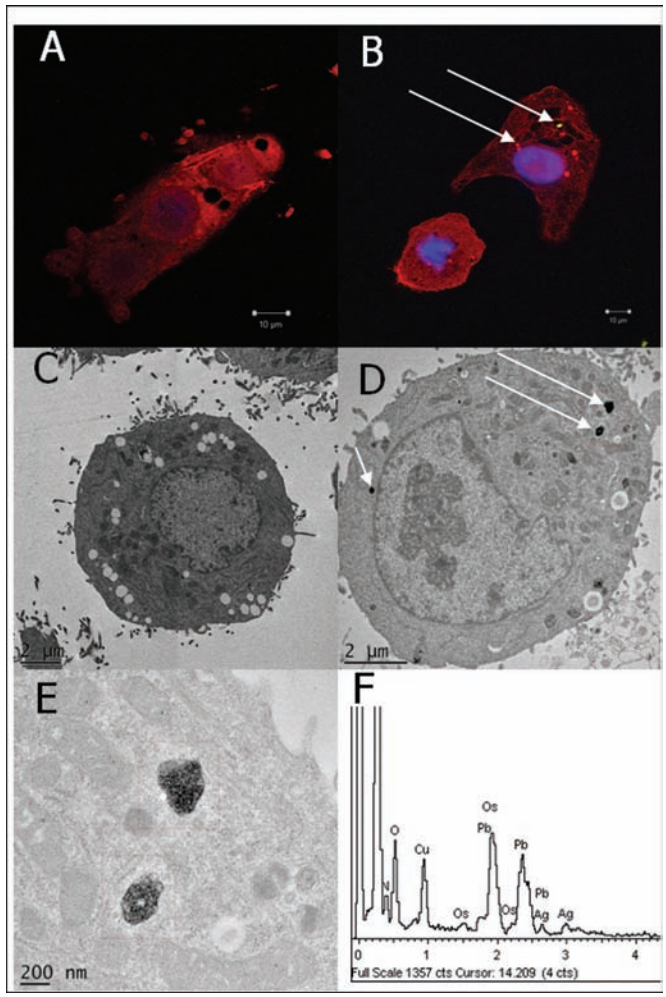

FIG. 2. C3A cells after exposure to NM300: Confocal images of C3A control cells (A) and cells exposed to 1 µg/cm² of NM300 for 24 h (B). Confocal images show the actin cytoskeleton, nuclei, and nanoparticle agglomerates, which appear as bright dots (arrows). Bars represent 10 µm. TEM images of control cell (C) and a cell exposed to 5 µg/cm² of NM300 for 4 h (D and E). Particle-filled vesicles are indicated with arrows (D) and showed close-up in (E). Bars represent 2 µm (C and D) and 200 nm (E). Particles were identified as Ag by EDX (F).

mitochondrial activity, and hence viability, of the cells. Using the AlamarBlue assay, we found an LC_{50} of approximately 20 µg/cm² (Fig. 1A). The results of the LDH assay suggest a higher toxicity, with an LC_{50} of approximately 2.5 µg/cm² (Fig. 1B). Exposure of cells to the equivalent volumes of the particle dispersant NM300-DIS did not cause any toxicity (Figs. 1A, B). To analyze whether C3A functionality was affected by Ag NPs, the supernatants of cells exposed to 1–4 µg/cm² of NM300 and NM300-DIS for 24 h, as well as 0.1% Triton-X100 and medium containing 0 and 20% FCS for influencing viability and functionality, were analyzed for albumin release from the cells. No significant decrease was found after exposure to the highest equivalent concentration of the dispersant (Fig. 1C). Ag at concentrations of 2 µg/cm² and higher significantly reduced albumin release into the medium (Fig. 1C). Adsorption of human albumin onto the particles was not observed at these concentrations. Reduction of albumin release was also measured with medium containing 0% FCS, which is nonlethal at 24 h of exposure but reduces cell functionality, and the cytotoxic Triton-X100 (Fig. 1C).

NP Uptake Into C3A Cells

Nanoparticle uptake into C3A cells was confirmed by confocal microscopy in cells exposed to 1 µg/cm² of NM300 for 24 h (Figs. 2A, B) and by TEM in cells exposed to 5 µg/cm² of NM300 for 4 h (Figs. 2C–E). Membrane-bound vesicles contained particles that were confirmed as Ag by EDX with characteristic bands at 2.7 and 3.0 keV (Fig. 2F).

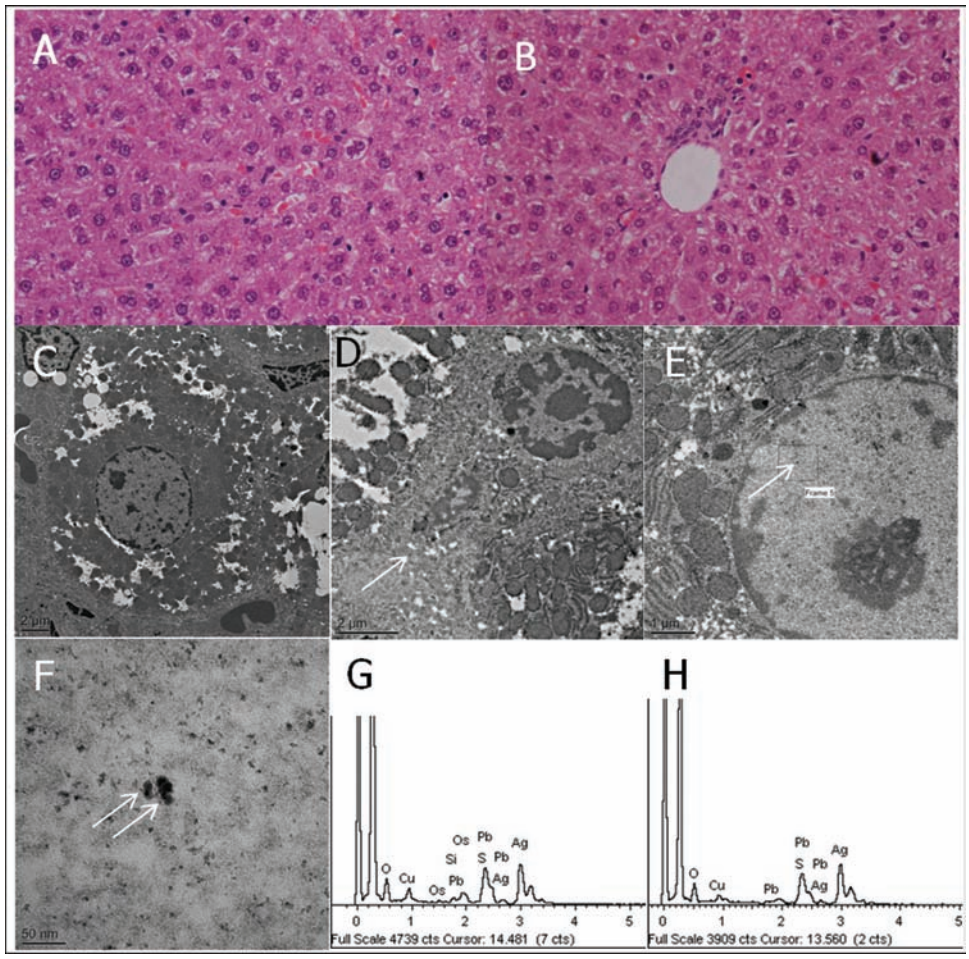

FIG. 3. Liver tissue following 24 h of exposure to 50 µg of dispersant and Ag NPs. Figure shows H&E-stained liver sections (×40) of control animals (A) and Ag-exposed livers (B). TEM sections show hepatocytes of control animals (C) and Ag-exposed animals (D–F). Arrows in (D–F) indicate location of NP aggregates. Bars represent 2 µm (C and D), 1 µm (E), and 50 nm (F). EDX spectra show characteristic bands for Ag in particle aggregates found in the cytoplasm (G) and the nucleus (H).

Histology and Transmission Electron Microscopy of Liver Tissue Following Ag Exposure

H&E-stained liver sections of control animals (Fig. 3A) and those exposed to 50 µg of iv administration of Ag NPs (Fig. 3B) appeared normal, and no particles were visible under the light microscope. Small particle aggregates were visible using TEM and were localized in the cytoplasm (Fig. 3D) and the nucleus (Figs. 3E, F).

Particle location was confirmed to be within the section by their Fresnel fringes, standing wave interference patterns occurring when electron microscopy images are defocused. Objects within the section will acquire Fresnel fringes at the same defocusing value, whereas objects deposited outside the plane of the section will acquire Fresnel fringes at a different defocusing value compared with those in the section (Stern *et al.*, 2012).

NPs were identified as Ag using EDX (bands at 2.7 and 3.0 keV, Figs. 3G, H). No membranes surrounding the particles were identified.

GSH Levels In Vitro *and* In Vivo

Levels of reduced GSH were measured in C3A cells after 2, 6, and 24 h of exposure to 1, 2, and 4 µg/cm^2 of Ag NPs and the positive *in vitro* control 0.5mM copper sulfate (Fig. 4A). We found no changes in GSH levels at either concentration or time point. Similarly, in livers of rats exposed to iv administration of 50 µg of Ag NPs and dispersant, no significant changes in GSH could be detected 24 h after exposure (Fig. 4B).

mRNA Expression Following Ag NP Exposure of C3A Cells

Further, mRNA expression of the inflammatory mediators IL-1β, IL-8, IL-10, TNF-α, MCP-1, and the IL-1 type I receptor (IL-1RI) was assessed by RT-PCR following 4 and 24 h of incubation to 0.1, 0.5, and 1 µg/cm^2 of NM300 and 1 µg/cm^2 NM300-DIS as a control. Levels of IL-1β, IL-10, and MCP-1 mRNA were below the detection limit of 40 cycles for all samples. IL8 expression relative to the control was increased at both time points and at all concentrations, with the exception

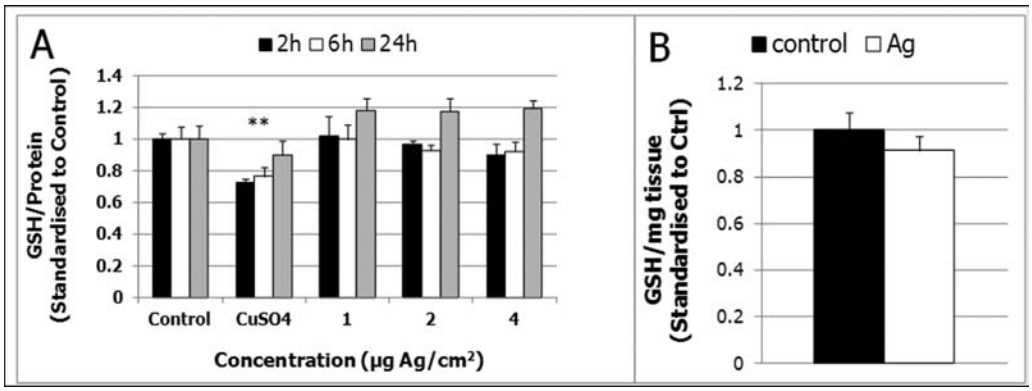

FIG. 4. Reduced GSH quantitation in C3A cells following exposure to 1, 2, and 4 µg/cm² of Ag NPs for 2, 6, and 24 h (A) and in rat liver 24 h after injection of 50 µg of Ag NPs into the tail vein. Values are normalized by milligrams of protein (cells) or tissue (livers) and standardized to the control. Bars represent means + SEM; $n = 3$, $^{**}p < 0.01$ (ANOVA followed by *t*-test).

of 0.5 µg/cm² of Ag after 24 h (Fig. 5A). IL1RI expression was unchanged, except for the lowest concentration (0.1 µg/cm²) after 24 h (Fig. 5B). TNF-α expression was increased after exposure to 0.1 µg/cm² of Ag at both time points but decreased at 1 µg/cm² after 4 h (Fig. 5C).

mRNA Expression in Rat Liver Following iv Ag NP Application

Analysis of mRNA expression in rat liver 24 h after iv injection of 50 µg of NM300 and NM300-DIS showed an increase in IL-1RI, MIP-2, and TNF-α expression (Fig. 6). No significant changes were detected in the expression of IL-1β, IL-10, MCP-1, and FasL and GSHpox.

Quantification of Inflammatory and Apoptotic Mediators Released From C3A Cells

We analyzed release of IL-8, TNF-α, FasLigand, and ICAM-1 from C3A cells 4 and 24 h after exposure to NM300 and NM300-DIS. TNF-α and FasL release were below the detection limit across the range of Ag concentrations used and at both time points. Both ICAM-1 and IL-8 release were increased after 4 h at the highest concentration of Ag used (40 µg/cm², Fig. 7A) and at concentrations of 5 µg/cm² or higher after 24 h (Fig. 7B). No changes were observed following exposure to NM300-DIS.

DISCUSSION

NM300 Ag NPs were highly cytotoxic in C3A cells at 24 h, as determined by LDH (LC_{50}, 2.5 µg/cm²) and AlamarBlue (LC_{50}, 20 µg/cm²) assays. These data confirm findings by Kermanizadeh *et al*. (2012), who used the same Ag particles for 24 h but analyzed toxicity using the WST-1 assay (LC_{50} approximately 2 µg/cm²). Although other Ag NPs have also been demonstrated to be highly toxic to hepatocyte cell lines and primary cells (Gaiser *et al*., 2012; Piao *et al*., 2011), to our knowledge this is the first report showing a decrease in albumin production in response to Ag NPs, suggesting that albumin release can be used as a marker of adverse effects of these NPs. Albumin is downregulated in the acute-phase response to a number of stresses, including inflammation (Sharma *et al*., 1992), and is a marker of liver function (Hasch *et al*., 1967).

One mechanism often suggested to be responsible for the toxicity of Ag NPs is oxidative stress (Carlson *et al*., 2008; Piao *et al*., 2011). We measured GSH depletion in both rat liver and C3A hepatocytes following exposure to Ag NPs but did not find significant changes. These findings contradict those of Piao *et al*. (2011), which showed a strong decrease in reduced GSH in human Chang hepatocytes treated with Ag NPs. This contradiction could be due to the type of Ag NPs used and a comparatively low release of Ag^+ ions (see Kermanizadeh *et al*. [2012]) but is also likely to be linked to Piao *et al*. (2011) using Ag NPs at a toxic dose, as evidenced by the images with rounded off, detaching cells at the concentrations used, whereas this study only used sublethal particle concentrations.

Following *in vitro* and *in vivo* exposure, NPs were readily taken up by hepatocytes and Kupffer cells. In the *in vitro* experiments, Ag NPs were concentrated within membrane-bound vesicles of 200–400 nm diameter. This indicates either effective removal from the cytoplasm after diffusion through the membrane and incorporation into phagosomes or lysosomes, or uptake by mechanisms involving membrane incorporation of particles (e.g., endocytosis). Particle aggregates were large enough to be visible by confocal microscopy. In contrast, *in vivo*, we found smaller agglomerates of less than 10 Ag particles in the cytoplasm, which were not visible under the light microscope and did not appear to be membrane bound. The presence of Ag NPs in the nucleus suggests that at least some of the particles were initially free within the cytoplasm.

In a separate study, following iv injection of gold NPs into Wistar rats, more than 90% of particles 5 nm or larger were retained in the liver for at least 24 h (Hirn *et al*., 2011). Sadauskas *et al*. (2007) showed that Kupffer cells are essential

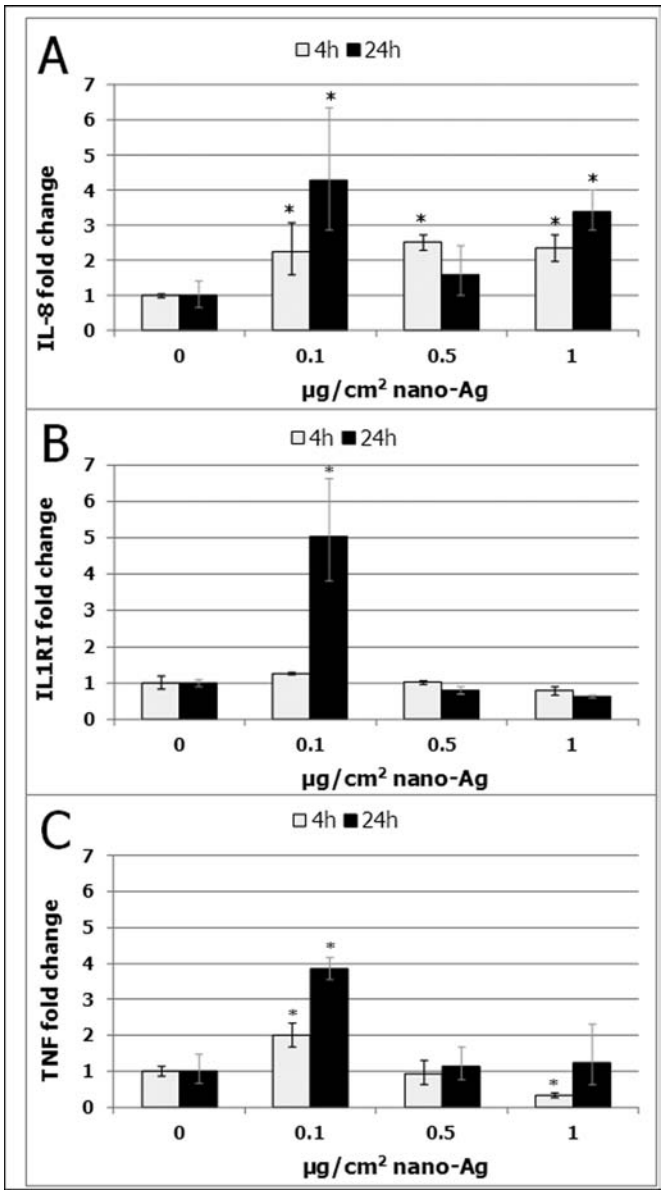

FIG. 5. Expression of mRNAs of inflammatory cytokines and receptors in C3A cells. Cells were exposed to sublethal concentrations of Ag NPs for 4 and 24 h, and mRNA expression of IL-8 (A), IL-1RI (B), and TNF-α (C) was analyzed by RT-PCR with GAPDH as an endogenous control. Bars represent expression relative to the dispersant control; error bars represent minimum and maximum expression. * describes expression changes 1.8-fold or higher with no overlaps with the control samples. $n = 3$.

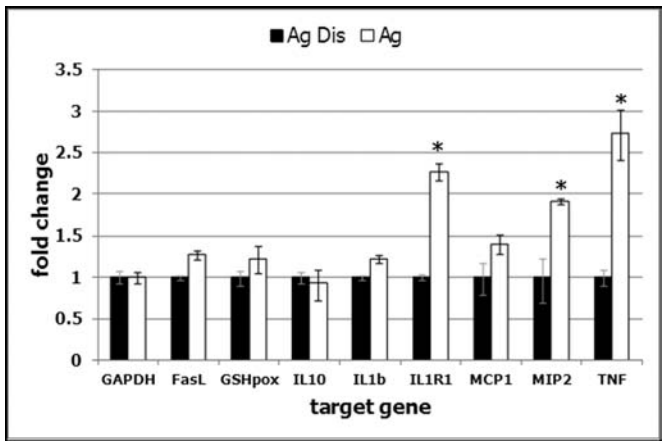

FIG. 6. Expression of mRNAs of inflammatory cytokines and receptors, FasL, and GSHpox in rat liver. Female Wistar rats were exposed to 50 µg Ag NPs for 24 h by injection via the tail vein, and mRNA expression was analyzed by RT-PCR with GAPDH as an endogenous control. Bars represent expression relative to the control exposed to the NP dispersant; error bars represent minimum and maximum expression. * describes expression changes 1.8-fold or higher with no overlaps with the control samples. $n = 3$.

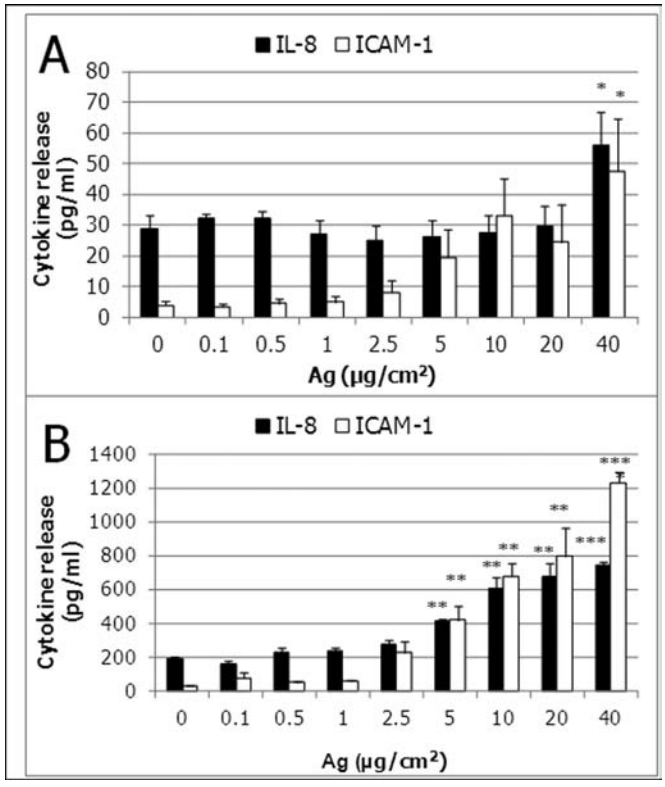

FIG. 7. IL-8 and ICAM-1 release from C3A cells exposed to 0–40 µg/cm² of NM300 for 4 (A) and 24 h (B). Bars represent means ($n = 3$) of cytokine concentrations in cell culture medium + SEM. *$p < 0.05$, **$p < 0.01$, ***$p < 0.001$.

for particle removal following iv administration. It is, therefore, likely that despite the majority of the injected dose still being present in the liver after 24 h, only a small percentage of the NPs would be found within hepatocytes rather than in Kupffer cells. In addition, it can be expected that the exposure of C3A cells to NPs under static conditions, rather than to particles distributed via the bloodstream, would encourage prolonged contact between particles and particle aggregates with the cell surface and, therefore, initiation of endocytotic or pinocytotic uptake mechanisms.

Uptake into the nucleus has been previously reported for Ag NPs in human bronchial epithelial BEAS-2B cells and was

associated with genotoxicity (Kim *et al*., 2011). Functionalized NPs are currently under review for targeting the nuclei of cancer cells (Ryou *et al*., 2011). However, studies with evidence of NP uptake into the nucleus are usually *in vitro* studies, as reviewed for gold NPs by Alkilany and Murphy (2010), and the fact that physiologically relevant doses of Ag NPs injected *in vivo* can lead to NPs passing through the nuclear barrier is a cause for concern for the development of nanomedicines and for particles translocating to the bloodstream following ingestion or inhalation.

IL-8 is an inflammatory cytokine involved in priming and attracting neutrophils, and an increase in IL-8 release has been observed in a number of cell systems and organs following particle exposure (Kermanizadeh *et al*., 2012; Salvi *et al*., 2000). We examined IL-8 mRNA and protein levels *in vitro* and expression of rodent MIP-2, one of the functional homologues of IL-8 (Tekamp-Olson *et al*., 1990), *in vivo*. We found a time- and concentration-dependent increase in IL-8 release from the C3A cell line. After 4 h, IL-8 mRNA expression was increased at doses as low as 0.1 μg/cm^2 of Ag but only apparent on the protein level at a very high NP concentration (40 μg/cm^2). After 24 h, IL-8 mRNA levels in C3A cells and MIP-2 levels in livers were still increased, and elevated levels of IL-8 in the cell culture medium were present at concentrations above 5 μg/cm^2. As the Ag NP concentration increased to doses of high toxicity, a plateau in IL-8 release was reached.

TNF-α gene expression was upregulated *in vivo* 24 h after exposure to Ag NPs and *in vitro* at the lowest concentration used, 0.1 μg/cm^2, at the 4 and 24 h time point. As the concentration of Ag increased, TNF-α gene expression in C3A cells decreased to or below control levels (0.5 or 1 μg/cm^2, respectively). These changes did, however, not translate on the protein level, where TNF-α release remained below detection over a wide range of Ag concentrations. Similarly, despite high levels of cell death, Fas ligand was undetectable in the medium, and another apoptosis kit used (annexin V) did not detect evidence of apoptosis in the C3A cells (data not shown). TNF-α expression is usually higher in inflammatory cells than in epithelium, and even though TNF-α release from primary hepatocytes has been demonstrated (dos Santos *et al*., 2011), we were unable to identify evidence for TNF-α release from C3A cells in the literature. It has also been shown that TNF-α is linked to apoptosis in the liver (Rimkunas *et al*., 2009), and it is possible that these pathways are not functional in C3A, a cancer cell line, or that the presence of inflammatory cells is required to induce a response similar to the *in vivo* situation.

The increase in expression of IL-1RI, but not IL-1β, in response to Ag NP exposure was surprising, as IL-1β is often involved in inflammatory processes. For example, Trickler *et al*. (2010) found IL-1β protein upregulation in a model of inflammation of the blood-brain barrier in response to Ag NPs, and Yazdi *et al*. (2010) detected increased levels of IL-1β gene expression in a model of pulmonary inflammation following exposure to nano-TiO_2. However, Yazdi *et al*. (2010) also stressed the dependence of the inflammatory reaction observed on IL-1RI signaling.

A common problem and topic of debate in *in vitro* nanotoxicology is the choice of the right model systems, time points, and also NP concentrations (e.g., Oberdörster [2012]). Although in our studies inflammatory mediator release into cell culture medium was increased from 5 μg/cm^2 of Ag NPs and higher, gene transcription was increased at much lower doses of 0.1 μg/cm^2. Indeed, the expression profile 24 h after exposure showed the best overlaps between the *in vitro* and *in vivo* models at this low dose. Therefore, we stress the importance of examining the adverse effects of NPs at low, noncytotoxic but more physiologically relevant doses *in vitro*.

ICAM-1 is a molecule involved in attraction and adhesion of inflammatory cells to endothelial and epithelial cells, and its soluble form, sICAM-1, is linked to activation of these cells in pathological responses (Gearing *et al*., 1992). sICAM-1 was increased in a mouse model following sc injection of nano-TiO_2 (Gonçalves and Girard, 2011) and following silica NP exposure of an *in vitro* model of the air-blood barrier (Kasper *et al*., 2011). Despite the absence of leukocytes in our *in vitro* model, we found an increase in sICAM-1 at the same concentrations of Ag NP exposure as the increase in IL-8 release, indicating hepatic inflammation and leukocyte signaling in response to Ag NPs.

C3A cells are a human hepatoma cell line and an established model of hepatocyte culture. Although they do not possess full capacity for metabolic processes such as cytochrome P450–mediated oxidation, these processes are not particularly significant for the toxicology of NPs. A comparative study between primary hepatocytes and C3A cells has recently been finished (Kermanizadeh *et al.*, in press) and found no significant differences between the response of primary cells and C3A cells to the materials examined here. Cocultures using Kupffer cells and hepatocytes have also been exposed to NPs in our group (Filippi *et al.*, in preparation). Although some responses such as cytokine release were different from the single-cell exposures, the coculture system presents methodological problems for the purpose of NP screening: Because no Kupffer cell line is available, the cultures involve animal experimentation, which is timely and costly, and replacement of which was one of the aims of this study as outlined in the abstract.

The main advantage of the tail vein exposure route is that the dose reaching the blood stream, and the liver, can be controlled and replicated between the animals in the exposure group. Furthermore, NP translocation into the blood can also occur via different routes, such as burn treatments on damaged skin and inhalation, so that initially it is desirable to determine the response to a known dose of NPs reaching the blood by any possible route. A disadvantage of the injection study is directly related to its advantage, namely that it is not sufficient to model the actual uptake of particles from the gut, lung, or damaged skin, and how these particles are changed or modified when translocating into the bloodstream.

The increasing production and use and the resulting exposure of humans to NPs via food and cosmetics, in an occupational setting or as medicines, makes it necessary to find suitable *in vitro* testing strategies to cope with the safety assessment of the increasing number of NPs entering the market. Uptake via the food and subsequent adverse effects are currently difficult to model and depend on a number of factors such as the matrix the particles are embedded in, eating habits, and the pH in the gastrointestinal tract, not least particle translocation.

The C3A model is a simplified model, in which the transport of NPs through the body and interaction with proteins and other substances in the blood or the gastrointestinal tract are not reflected. The liver has been identified as a target organ following particle uptake via routes such as ingestion, inhalation, and dermal exposure. Investigation of the effects of a known amount of NPs entering the bloodstream and reaching the liver, and finding suitable *in vitro* models, is therefore step toward animal replacement for NP safety testing and contributes to projects such as InLiveTox, as part of which this study was conducted, and which aim to establish more complex multicompartment models for safety testing. Therefore, C3A culture provides very important information, with relevant similarities to the *in vivo* model, on the way to models that are hopefully more sophisticated and physiological while still being suited to medium- to high-throughput screening.

In addition, the application of NPs straight to the bloodstream, e.g., for imaging purposes or as adjuvans, is expected to play an increasing role in the growing field of nanomedicine, and a direct, high exposure of the liver via the blood is very likely. Therefore, the results in this study could also be used to inform safety testing of nanomedicines.

In conclusion, Ag NPs induced inflammation and toxicity not associated with GSH depletion in acute exposure liver models *in vitro* and *in vivo*. The simple hepatocytes model used was adequate to mirror many of the *in vivo* responses following iv injection, though choice of time point and concentration of NP suspensions were essential. We are hoping that the results will contribute to safer design and efficient risk management of NPs and advanced *in vitro* testing strategies and models and to reduction of animal use in NP risk assessment.

FUNDING

European Union's 7th Framework Programme InLiveTox and ENPRA (NMP4-SL-2009–228625, NMP4-SL-2009–228789).

ACKNOWLEDGMENTS

The authors would like to thank Dr Steve Mitchell (University of Edinburgh) for TEM sample preparation, Dr Michael Ward and the Leeds EPSRC Nanoscience and Nanotechnology Facility (LENNF) for TEM imaging, Dorinda Wright (Histologix Ltd.) for preparation of the histological specimens, Nadine Senger and Sebastian Kaidel (Helmholtz Centre Munich) for the technical assistance, and Giulio Pojana and Antonio Marcomini (University Ca' Foscari, Venice) for particle characterization.

REFERENCES

Alkilany, A. M., and Murphy, C. J. (2010). Toxicity and cellular uptake of gold nanoparticles: What we have learned so far? *J. Nanopart. Res.* **12,** 2313–2333.

Bradford, M. M. (1976). A rapid and sensitive method for the quantitation of microgram quantities of protein utilizing the principle of protein-dye binding. *Anal. Biochem.* **72,** 248–254.

Brown, D. M., Wilson, M. R., MacNee, W., Stone, V., and Donaldson, K. (2001). Size-dependent proinflammatory effects of ultrafine polystyrene particles: A role for surface area and oxidative stress in the enhanced activity of ultrafines. *Toxicol. Appl. Pharmacol.* **175,** 191–199.

Carlson, C., Hussain, S. M., Schrand, A. M., Braydich-Stolle, L. K., Hess, K. L., Jones, R. L., and Schlager, J. J. (2008). Unique cellular interaction of silver nanoparticles: Size-dependent generation of reactive oxygen species. *J. Phys. Chem. B* **112,** 13608–13619.

Chao, J. B., Liu, J. F., Yu, S. J., Feng, Y. D., Tan, Z. Q., Liu, R., and Yin, Y. G. (2011). Speciation analysis of silver nanoparticles and silver ions in antibacterial products and environmental waters via cloud point extraction-based separation. *Anal. Chem.* **83,** 6875–6882.

Cheng, C., Yun, K.-Y., Ressom, H. W., Mohanty, B., Bajic, V. B., Jia, Y., Yun, S. J., and de los Reyes, B. G. (2007). An early response regulatory cluster induced by low temperature and hydrogen peroxide in seedlings of chilling-tolerant japonica rice. *BMC Genomics* **8,** 175.

dos Santos, S. A., de Andrade Júnior, D. R., and de Andrade, D. R. (2011). TNF-α production and apoptosis in hepatocytes after Listeria monocytogenes and Salmonella Typhimurium invasion. *Rev. Inst. Med. Trop. Sao Paulo* **53,** 107–112.

Gaiser, B. K., Fernandes, T. F., Jepson, M. A., Lead, J. R., Tyler, C. R., Baalousha, M., Biswas, A., Britton, G. J., Cole, P. A., Johnston, B. D., *et al.* (2012). Interspecies comparisons on the uptake and toxicity of silver and cerium dioxide nanoparticles. *Environ. Toxicol. Chem.* **31,** 144–154.

Gearing, A. J., Hemingway, I., Pigott, R., Hughes, J., Rees, A. J., and Cashman, S. J. (1992). Soluble forms of vascular adhesion molecules, E-selectin, ICAM-1, and VCAM-1: Pathological significance. *Ann. N. Y. Acad. Sci.* **667,** 324–331.

Gonçalves, D. M., and Girard, D. (2011). Titanium dioxide (TiO2) nanoparticles induce neutrophil influx and local production of several pro-inflammatory mediators in vivo. *Int. Immunopharmacol.* **11,** 1109–1115.

Hasch, E., Jarnum, S., and Tygstrup, N. (1967). Albumin synthesis rate as a measure of liver function in patient with cirrhosis. *Acta Med. Scand.* **182,** 83–92.

Hirn, S., Semmler-Behnke, M., Schleh, C., Wenk, A., Lipka, J., Schäffler, M., Takenaka, S., Möller, W., Schmid, G., Simon, U., *et al.* (2011). Particle size-dependent and surface charge-dependent biodistribution of gold nanoparticles after intravenous administration. *Eur. J. Pharm. Biopharm.* **77,** 407–416.

Johnston, H. J., Hutchison, G., Christensen, F. M., Peters, S., Hankin, S., and Stone, V. (2010). A review of the in vivo and in vitro toxicity of silver and gold particulates: Particle attributes and biological mechanisms responsible for the observed toxicity. *Crit. Rev. Toxicol.* **40,** 328–346.

Kasper, J., Hermanns, M. I., Bantz, C., Maskos, M., Stauber, R., Pohl, C., Unger, R. E., and Kirkpatrick, J. C. (2011). Inflammatory and cytotoxic responses of an alveolar-capillary coculture model to silica nanoparticles: Comparison with conventional monocultures. *Part. Fibre Toxicol.* **8,** 6.

Kermanizadeh, A., Pojana, G., Gaiser, B. K., Birkedal, R., Bilanicova, D., Wallin, H., Jensen, K. A., Sellergren, B., Hutchison, G. R., Marcomini, A., *et al.* (2012). In vitro assessment of engineered nanomaterials using a hepatocyte cell line: Cytotoxicity, pro-inflammatory cytokines and functional markers. *Nanotoxicology*. Advance access published January 20, 2012. doi:10.3109/17435390.2011.653416.

Kim, H. R., Kim, M. J., Lee, S. Y., Oh, S. M., and Chung, K. H. (2011). Genotoxic effects of silver nanoparticles stimulated by oxidative stress in human normal bronchial epithelial (BEAS-2B) cells. *Mutat. Res.* **726,** 129–135.

Klein, C., Comero, S., Stahlmecke, B., Romazanov, J., Kuhlbusch, T., van Doren, E., Wick, P., Locoro, G., Koerdel, W., Gawlik, B., *et al.* (2011). NM-300 silver characterisation, stability, homogeneity. EUR – Scientific and Technical Research Reports, JRC Publication No. JRC60709, EUR 24693 EN, Publications Office of the European Union. Doi:10.2788/23079.

Korani, M., Rezayat, S. M., Gilani, K., Arbabi Bidgoli, S., and Adeli, S. (2011). Acute and subchronic dermal toxicity of nanosilver in guinea pig. *Int. J. Nanomedicine* **6,** 855–862.

Kulthong, K., Srisung, S., Boonpavanitchakul, K., Kangwansupamonkon, W., and Maniratanachote, R. (2010). Determination of silver nanoparticle release from antibacterial fabrics into artificial sweat. *Part. Fibre Toxicol.* **7,** 8.

Mühlfeld, C., Gehr, P., and Rothen-Rutishauser, B. (2008). Translocation and cellular entering mechanisms of nanoparticles in the respiratory tract. *Swiss Med. Wkly.* **138,** 387–391.

Nishanth, R. P., Jyotsna, R. G., Schlager, J. J., Hussain, S. M., and Reddanna, P. (2011). Inflammatory responses of RAW 264.7 macrophages upon exposure to nanoparticles: Role of ROS-NFκB signaling pathway. *Nanotoxicology* **5,** 502–516.

Nowack, B., Krug, H. F., and Height, M. (2011). 120 years of nanosilver history: Implications for policy makers. *Environ. Sci. Technol*. Advance access published January 10, 2011. doi:10.1021/es103316q.

Oberdörster, G. (2012). Nanotoxicology: In vitro-in vivo dosimetry. *Environ. Health Perspect.* **120,** A13.

Piao, M. J., Kang, K. A., Lee, I. K., Kim, H. S., Kim, S., Choi, J. Y., Choi, J., and Hyun, J. W. (2011). Silver nanoparticles induce oxidative cell damage in human liver cells through inhibition of reduced glutathione and induction of mitochondria-involved apoptosis. *Toxicol. Lett.* **201,** 92–100.

Powers, C. M., Badireddy, A. R., Ryde, I. T., Seidler, F. J., and Slotkin, T. A. (2011). Silver nanoparticles compromise neurodevelopment in PC12 cells: Critical contributions of silver ion, particle size, coating, and composition. *Environ. Health Perspect.* **119,** 37–44.

Rimkunas, V. M., Graham, M. J., Crooke, R. M., and Liscum, L. (2009). TNF-{alpha} plays a role in hepatocyte apoptosis in Niemann-Pick type C liver disease. *J. Lipid Res.* **50,** 327–333.

Ryou, S. M., Kim, J. M., Yeom, J. H., Hyun, S., Kim, S., Han, M. S., Kim, S. W., Bae, J., Rhee, S., and Lee, K. (2011). Gold nanoparticle-assisted delivery of small, highly structured RNA into the nuclei of human cells. *Biochem. Biophys. Res. Commun.* **416,** 178–183.

Sadauskas, E., Wallin, H., Stoltenberg, M., Vogel, U., Doering, P., Larsen, A., and Danscher, G. (2007). Kupffer cells are central in the removal of nanoparticles from the organism. *Part. Fibre Toxicol.* **4,** 10.

Salvi, S. S., Nordenhall, C., Blomberg, A., Rudell, B., Pourazar, J., Kelly, F. J., Wilson, S., Sandström, T., Holgate, S. T., and Frew, A. J. (2000). Acute exposure to diesel exhaust increases IL-8 and GRO-alpha production in healthy human airways. *Am. J. Respir. Crit. Care Med.* **161**(2 Pt 1), 550–557.

Schleh, C., Semmler-Behnke, M., Lipka, J., Wenk, A., Hirn, S., Schäffler, M., Schmid, G., Simon, U., and Kreyling, W. G. (2012). Size and surface charge of gold nanoparticles determine absorption across intestinal barriers and accumulation in secondary target organs after oral administration. *Nanotoxicology* **6,** 36–46.

Senft, A. P., Dalton, T. P., and Shertzer, H. G. (2000). Determining glutathione and glutathione disulfide using the fluorescence probe o-phthalaldehyde. *Anal. Biochem.* **280,** 80–86.

Sharma, R. J., Macallan, D. C., Sedgwick, P., Remick, D. G., and Griffin, G. E. (1992). Kinetics of endotoxin-induced acute-phase protein gene expression and its modulation by TNF-alpha monoclonal antibody. *Am. J. Physiol.* **262**(5 Pt 2), R786–R793.

Silver, S., Phung, le. T., and Silver, G. (2006). Silver as biocides in burn and wound dressings and bacterial resistance to silver compounds. *J. Ind. Microbiol. Biotechnol.* **33,** 627–634.

Stern, A., Rotem, D., Popov, I., and Porath, D. (2012). Quasi 3D imaging of DNA-gold nanoparticle tetrahedral structures. *J. Phys. Condens. Matter* **24,** 164203.

Stone, V., Johnston, H., and Schins, R. P. (2009). Development of in vitro systems for nanotoxicology: Methodological considerations. *Crit. Rev. Toxicol.* **39,** 613–626.

Tekamp-Olson, P., Gallegos, C., Bauer, D., McClain, J., Sherry, B., Fabre, M., van Deventer, S., and Cerami, A. (1990). Cloning and characterization of cDNAs for murine macrophage inflammatory protein 2 and its human homologues. *J. Exp. Med.* **172,** 911–919.

Trickler, W. J., Lantz, S. M., Murdock, R. C., Schrand, A. M., Robinson, B. L., Newport, G. D., Schlager, J. J., Oldenburg, S. J., Paule, M. G., Slikker, W., Jr, *et al.* (2010). Silver nanoparticle induced blood-brain barrier inflammation and increased permeability in primary rat brain microvessel endothelial cells. *Toxicol. Sci.* **118,** 160–170.

Wong, K. K., Cheung, S. O., Huang, L., Niu, J., Tao, C., Ho, C. M., Che, C. M., and Tam, P. K. (2009). Further evidence of the anti-inflammatory effects of silver nanoparticles. *ChemMedChem* **4,** 1129–1135.

Yazdi, A. S., Guarda, G., Riteau, N., Drexler, S. K., Tardivel, A., Couillin, I., and Tschopp, J. (2010). Nanoparticles activate the NLR pyrin domain containing 3 (Nlrp3) inflammasome and cause pulmonary inflammation through release of IL-1α and IL-1β. *Proc. Natl. Acad. Sci. U.S.A.* **107,** 19449–19454.